Title

A search for evidence of strain gradient hardening in Au submicron pillars under uniaxial compression using synchrotron X-ray microdiffraction

Journal

Acta Materialia, 56(3)

ISSN

1359-6454

Authors

Budiman, A.S.
Han, S.M.
Tamura, N.
et al.

Publication Date

2008-02-28

A SEARCH FOR EVIDENCE OF STRAIN GRADIENT HARDENING IN Au SUBMICRON PILLARS UNDER UNIAXIAL COMPRESSION USING SYNCHROTRON X-RAY MICRODIFFRACTION

A. S. BUDIMAN[1], S.M. HAN[1], J.R. GREER[2], N. TAMURA[3], J.R. PATEL[†1,3], W. D. NIX[1]

[1]Department of Materials Science & Engineering, Stanford University, Stanford, CA 94305;

[2]Palo Alto Research Center (PARC), Palo Alto, CA 94034;

[3]Advanced Light Source (ALS), Lawrence Berkeley National Laboratory (LBNL), CA 94720

ABSTRACT

When crystalline materials are mechanically deformed in small volumes, higher stresses are needed for plastic flow. This has been called the "Smaller is Stronger" phenomenon and has been widely observed. Various size-dependent strengthening mechanisms have been proposed to account for such effects, often involving strain gradients. Here we report on a search for strain gradients as a possible source of strength for single-crystal submicron pillars of gold subjected to uniform compression, using a submicron white-beam (Laue) x-ray diffraction technique. We have found both before and after uniaxial compression, no evidence of either significant lattice curvature or sub-grain structure. This is true even after 35% strain and a high flow stress of 300 MPa were achieved during deformation. These observations suggest that plasticity here is not controlled by strain gradients or sub-structure hardening, but rather by dislocation source starvation, wherein smaller volumes are stronger because fewer sources of dislocations are available.

Keywords: Materials with reduced dimensions; Size effects; Dislocation, Synchrotron radiation; X-ray diffraction (XRD)

INTRODUCTION

Investigations of the role of length-scales in the mechanical behavior of materials have great importance to the field of materials science, especially in today's nano-age where sub-micron and nanoscale devices are built near the size of their microstructural features. The creation of such small components requires a thorough understanding of the mechanical properties of materials at these small length scales. In the macroscale (bulk), the mechanical properties of materials are commonly described by single valued parameters (eg. yield stress, hardness, etc), which are largely independent of the size of the specimen. However, as specimens are reduced in size to the scale of the microstructure, their mechanical properties deviate from those of bulk materials. For example, in thin films – where only one dimension, the thickness, reaches the micron scale and below – the flow stress is found to be higher than its bulk value, and becomes even higher as the film gets thinner. This size effect is usually attributed to the confinement of dislocations by the substrate[1-3].

In nanoindentation experiments, where the length-scale of the deformation reaches the microstructural length-scale of the material, the governing relations between stress and strain deviate from the classical laws that apply to bulk materials. At small depths of indentation the hardness of crystalline materials is usually higher than that of large indentations. This indentation size effect (ISE) has been explained using the concept of geometrically necessary dislocations (GNDs) and strain gradients.[4-17] According to this picture, the hardness increases with decreasing

depth of indentation because the total length of geometrically necessary dislocations forced into the solid by the self-similar indenter scales with the square of the indentation depth, while the volume in which these dislocations are found scales with the cube of the indentation depth. This leads to a geometrically necessary dislocation density that depends inversely on the depth of indentation. The higher dislocation densities expected at smaller depths leads naturally to higher strengths through the Taylor relation, and this leads to the ISE.[18]

Recently Uchic et al.[19] and others[20,21] have shown that micro pillars of various metals with diameters in the micron range, subjected to uniaxial compression, are much stronger than bulk materials. For example, micro pillars of gold ranging in diameter between 200 nm and several microns have been found to have compressive flow strengths as high as 800 MPa, a value ~50 times higher than the strength of bulk gold.[20,21] However, in spite of much progress on size effects on strength there is still no unified theory for plastic deformation at the sub-micron scale. The accounts of strain gradient plasticity, as discussed above, appear to break down for the case of micro pillar compression because the deformation is essentially uniform.

Greer and Nix[21] suggested that the high strengths of sub-micron pillars of gold might be controlled by a dislocation starvation hardening process. In this mechanism and for small enough pillars, the mobile dislocations have a higher probability of annihilating at a nearby free surface than of multiplying and being pinned by other dislocations. When the starvation conditions are met, plasticity is accommodated by the nucleation and motion of new dislocations rather than by motion and interactions of existing dislocations, as in the case of bulk crystals.

While significant strain gradients are not expected to develop during the compression of micron sized pillars, there is very little experimental evidence to support this expectation. Since strain gradients and GNDs are directly related to the local lattice curvature, the technique of

Scanning X-ray Microdiffraction (μ-SXRD) using a focused polychromatic/white synchrotron x-ray beam can be used to determine the density of GNDs. This has proven to be useful in the study of the early stages of electromigration failure in interconnect lines, wherein lattice bending and GNDs are created by electromigration processes.[22-23] This capability is related to the continuous range of wavelengths in a white x-ray beam, allowing Bragg's Law to be satisfied even when the lattice is locally rotated or bent, resulting in the observation of streaked Laue spots.

Using this approach, we can monitor the change in the Laue diffraction peaks before and after uniaxial compression of a sub-micron single crystal Au pillar. A quantitative analysis of the Laue peak widths then allows us to estimate the density of GNDs in the pillar. The absolute number of geometrically necessary dislocations in the crystal can then be determined using the dimensions of the pillar. A comparison of the numbers of geometrically necessary dislocations before and after the uniaxial compression provides information about the change in microstructure associated with plastic deformation.

The technique of synchrotron-based white beam x-ray diffraction is one of the few methods for detecting and measuring the densities of GNDs in crystalline materials after deformation. Electron microscopy techniques, such as TEM, can also be used to detect presence of dislocations in small volumes, but the thinning required to obtain electron transparency could alter the defect structure being observed (dislocations may escape as the very thin crystal is cut from the pillar).

The synchrotron technique of scanning white beam x-ray microdiffraction has been described thoroughly elsewhere.[24] The power of this technique to study local plasticity and mechanical behavior of materials at small scales stems from the high brilliance of the

synchrotron source, as well as the recent advances in x-ray focusing optics (allowing sample mapping at the sub-micron level).

EXPERIMENTAL

The sample consists of a 4-crystal film of gold oriented <111> out-of-plane (Figure 1), and deposited onto a <001> chromium single crystal substrate, in the form of a 2 mm-thick, 10 mm-diameter disk. The native oxide on the surface of the Cr substrate was first removed by ion cleaning in a high vacuum, using the appearance of a RHEED pattern of single crystal Cr to indicate the removal of the surface oxide. A thin layer of gold was then epitaxially deposited onto the bare Cr surface by vapor deposition in the same high vacuum chamber, before moving the sample to a sputtering system to continue growth to a thickness of 1.9 μm. While a <001> orientation was expected for the gold film on the basis of interface energy considerations, the low energy of the (111) surface must have caused the <111> orientation to be selected. For this orientation, a nearly perfect lattice match is achieved along a <110> direction in the (111) surface of Au and a <100> direction in the (001) surface of Cr.

The pillars were fabricated utilizing the method of FIB machining, following the approach developed by Greer et al.[21] Circular craters 30 μm in diameter were first carved out of the gold film, leaving behind only the sub-micron pillars at the centers of the craters (Figure 2(a,b)). Using scanning electron microscopy, we determined that the Au pillar (Figure 2(c)) was a bicrystal of Au with top and bottom crystals having different in-plane orientations. The top crystal layer was about 1.1 μm in height and became the focus of our experiment. It has diameter of 0.58 μm leading to a height to diameter ratio of close to 2:1 for that crystal.

The uniaxial compression testing of these submicron pillars was conducted using an MTS Nanoindenter XP with a flat punch diamond tip, following the methodology described by Han.[25] The nanoindenter, which is a load-controlled instrument, was programmed to perform a nominally displacement-controlled test. In this method, the displacement rate is calculated continuously during the compression test, based on the measured displacement and time. When the measured displacement rate is below a specified value, the load is adjusted to maintain that particular displacement rate. This method is designed to simulate a constant displacement rate. Load-displacement data were collected in the continuous stiffness measurement (CSM) mode of the instrument. The data obtained during compression were then converted to uniaxial stresses and strains using the assumption that the plastic volume is conserved throughout this mostly-homogeneous deformation.

The white beam x-ray microdiffraction experiment (Figure 3) was performed on beamline 7.3.3. at the Advanced Light Source, Berkeley, CA. The sample was mounted on a precision XY Huber stage and the pillar of interest was raster scanned at room temperature under the x-ray beam before and after the uniaxial compression (*ex situ*); this provided X-Ray microFluorescence (μXRF) and X-Ray microDiffraction (μXRD) scans for the area near the pillar. The μXRD patterns were collected using a MAR133 X-ray CCD detector and analyzed using the XMAS software package.

The μXRF scan was conducted first for precise positioning of the Au pillar prior to the μXRD scan. The μXRF scan was made using 1 μm step sizes to cover a large area of typically 70 x 70 μm (to include not only the 30 μm diameter crater, but also the identifying mark – number "4" in Figure 1). The circular crater was used, first, to clearly locate the position of the pillar (as the pillar was fabricated at the center of the crater), and, secondly, to partially separate the

diffraction signal of the pillar from that of the surrounding gold film, such that only those diffracted beams from the pillar (and not those of the surrounding film) can be studied.

Once the Au pillar was located and identified, an μXRD scan was conducted to obtain diffraction data primarily from the Au crystal/pillar. The typical scan for this purpose was made with 1 μm step sizes, 50 steps across the diameter of the crater (50 μm scan length) and 10 steps along its orthogonal direction (10 μm scan length), making it a wide band of 50 x 10 μm. This scan area was designed to include not only the pillar, but also the boundaries of the crater with the surrounding Au film as positional references. This μXRD scan involved the collection of 500 CCD frames. A complete set of CCD frames took about 4 to 5 hours to collect. The exposure time was 5 s, in addition to about 10 s of electronic readout time for each frame.

With μXRD, we monitored the change in the Laue diffraction images before and after uniaxial compression of a single crystal submicron Au pillar. A quantitative analysis of the Laue peak widths allows us to estimate the density of GNDs in the submicron single crystal pillars. The exact geometries of the pillars being known, the absolute number of dislocations in the single crystal can be derived. A comparison of the numbers of dislocations before and after the uniaxial compression would unveil the change in the structure involved in the deformation.

RESULTS & DISCUSSION

Figure 4 shows the mapping of the $(\bar{3}11)$ Laue diffraction spot from the top crystal of the pillar with the incident x-ray beam located at various positions in the vicinity of the pillar and crater, before any compressive deformation. Here, and hereafter, all of our attention will be focused on the upper crystal in the Au pillar structure.

Each of the individual images of the Laue diffraction spots in Figure 4 represents a (diffracted) intensity contour in a 2-D χ -2θ coordinate system (i.e. the 2-D coordinate in the diffractometer coordinate system). For the undeformed pillar, the shapes of individual Laue diffraction spots from position to position are nominally the same, and are rounded in shape, as expected. However, as we set the threshold of the lower-bound intensity display to be the same for all images, the difference in peak size/width in the mapping indicates a difference in the absolute diffracted intensity of the Au crystal volume at a particular position in the map. Thus, the size of the red "dots" is directly related to the diffracted volume of Au crystal. The bigger red "dots" on the left-hand and right-hand sides of this map clearly represent the surrounding Au films, while the smaller red dots in the middle area represent the crater (close to zero diffracting volume). Obviously, as there is no Au crystal away from the center of the crater, there ought to be absolutely zero diffraction intensity in this area. However, because of the Lorentzian shape of the incoming focused X-ray beam, the tails of the beam extend beyond (up to tens of microns) the nominal FWHM (~1 um) of the beam. Therefore, even though the beam is focused on a particular location in the crater, there is still a very small fraction of diffraction intensity coming from the surrounding film picked up by the tails of the x-ray beam.

The diffraction map in Figure 4 also indicates unambiguously the exact location of the pillar itself (marked by the solid line box in Figure 4). After subtracting out the diffraction intensity by the tails of the x-ray beam, a significant diffraction intensity was still left on the location at the centre of the solid line box (ie. the pillar). This is so as there is indeed slightly more volume of Au crystal to diffract at the location of the pillar, but this intensity is not as high as in the surrounding film areas (thus the relative size of the peak). The location associated with

the slightly bigger Laue diffraction spot also coincides with the center of the crater as identified by dashed and dotted circle in the map of Figure 4.

Figure 5(a) shows the stress-strain curves of the 0.58-μm Au pillar obtained during the compression testing. Uniaxial loading in the <111> direction of the Au crystal/pillar, corresponding to a high-symmetry orientation, would result in the activation of multiple slip systems, with the pillar deforming uniformly around its diameter as it is compressed. The flow stress reaches value as high as 280 MPa. This is close to 10 times the yield stress of gold in bulk, and falls consistently in the flow stress vs. pillar diameter chart described by Greer and Nix.[21] In this <111> loading orientation, and despite the presence of the end constraints, the pillar remains centrally-loaded and preserves its cylindrical shape throughout the deformation process as shown in Figure 5(b). The final diameter of the pillar after the uniaxial compression is 0.67 μm, which represents a total strain of close to 35%.

A diffraction scan was again taken covering the deformed pillar and the surrounding area (including the crater border with the surrounding Au film) similarly to the diffraction map in Figure 4. Following the methodology described above, we again identify the location of the deformed pillar, and subsequently we select a particular Laue diffraction spot (in the case shown here, $(\bar{3}11)$ diffraction spot) associated with the location of the deformed pillar for further quantitative analysis and comparison. We subtracted the background intensity and checked that there is no Au crystal rotation involved (which would have manifested in the shift of the position of the Au Laue peak with respect to the Laue diffraction pattern of the chromium substrate reference), in order to be able to directly compare the $(\bar{3}11)$ Laue spots before and after deformation and infer what happened to the pillar crystal during the deformation process. Figure

6 shows the data of the pillar crystal (SEM images, Laue diffraction spots, and Intensity profiles) for both undeformed and deformed states side-by-side.

Figure 6(b) shows that both ($\bar{3}11$) Laue spots have the same shape and that they are both rounded – not broadened toward a certain direction (streaked). This rounded shape is typical of an undeformed crystal, whereas broadening of a Laue diffraction spot in a certain direction (streaking) would have been associated with the presence of strain gradients in the deformation volume. A more detailed treatment of the streak length and its correlation with the curved, or in general, plastically deformed crystal has been described elsewhere.[22-23]

The fact that the Laue diffraction spot in the deformed state is not streaked suggests that there is no strain gradient involved during the uniaxial compression of the pillar. Furthermore, as it shows neither a shift in the absolute position of the Laue spots, nor a split, we can further infer that there is no crystal rotation or polygonization (formation of subgrain structures) in the pillar crystal upon the deformation. This is an important observation considering the huge amount of strain (~35%) that the crystal underwent.

In Figure 6(c) we take the intensity traces along a particular χ to study the Laue diffraction peak profile more quantitatively. The profiles were fitted with Lorentzian curves. The measured FWHMs (full width half maximum) of both profiles show that there is an increase of 0.01º in the angular width. However, this difference is still well within the experimental error bar of the instrumentation[24] rendering the two measurements statistically identical. If this "broadening" of 0.01º in angle were real, it would only amount to a difference of up to 1.01/μm^2 in dislocation density (as calculated from the Cahn-Nye relationship[26-27] and taking the relevant dimensions of the pillar). This essentially means that within the volume of our pillar, there could only be no more than 2 additional same-sign dislocations after the deformation.

This observation is consistent with the earlier TEM observations on a deformed gold pillar conducted by Greer and Nix.[21] Their TEM results showed that there were only 2 dislocations left in their pillar after deformation and that they were both of a non-movable type for the uniaxial compressive loading of their experiment. Both observations (the present Laue x-ray microdiffraction and the earlier TEM results) support the idea that sub-micron single crystal gold pillars are nearly defect-free even after significant plastic deformation. This view was recently further supported by the *in situ* TEM observations of the compression of single crystal nickel pillars by Minor et al.[28] They found that the dislocations present in undeformed pillars (including some dislocation loops near the pillar surfaces created by FIB damage) quickly escaped from the pillar during compressive deformation, leaving the pillar free of dislocations after compression.

We may now conclude that the present white-beam x-ray microdiffraction observations, supported by the closely related TEM results,[21,28] are consistent with the model of hardening of small crystals by dislocation starvation and dislocation nucleation or source-controlled plasticity, as suggested by Greer and Nix.[21] In ordinary plasticity (ie. in typical, bulk samples), dislocation motion leads to dislocation multiplication by various cross-slip processes, invariably leading to softening before strain hardening occurs through elastic interaction of dislocations. However in small samples, such as the sub-micron Au single crystal pillar under study here, dislocations can travel only very small distances before annihilating at free surfaces, thereby reducing the overall dislocation multiplication rate. The central idea is that, as dislocations leave the crystal more frequently than they multiply, the crystal can quickly reach a dislocation-starved state. When such a state is reached, continued loading would force other, harder sources of dislocations to be activated in the crystal, leading to the abrupt rise in the measured flow stress (ie. hardening).

The Cahn-Nye relation that we have used to estimate the number of GNDs in the deformed crystal is based on same-signed dislocations in a single slip system. Yet multiple slip occurred in this pillar compression experiment. One model for lattice rotation produced by multiple slip systems, which leaves statistically-stored dislocations in the crystal, is shown in Figure 7(a). For this configuration, the lattice rotation, $\Delta\theta$, depends on the magnitude of the Burgers vector and the separation distance between dislocations, s, as shown in the Figure 7(a). Once again, if the observed "broadening" of 0.01º in angle were real, it would amount to a lattice rotation of 0.01º, which would give a spacing between dislocations, s, of 1.7 μm. Considering the dimensions of the pillar crystal of interest (which is the "Au upper crystal" in Figure 7(b)), this essentially means that within the volume of our pillar, there could not be such cell of statistically-stored edge dislocations. This calculation further confirms that the pillar crystal is essentially left defect-free after the deformation.

CONCLUSIONS

Using synchrotron white-beam x-ray sub-micron diffraction, we have studied a submicron single crystal Au pillar, before and after uniaxial plastic deformation, and found no evidence of measurable lattice rotation or lattice curvature caused by the deformation, even though a plastic strain of about 35% was imposed and a high flow stress of close to 300 MPa was achieved in the course of deformation. These observations, coupled with other examinations using electron microscopy, suggest that plasticity here is not controlled by strain gradients, but rather by dislocation source starvation, with smaller volumes being stronger because fewer sources of dislocations are available. The central idea of this model is that for very small crystals,

dislocations leave the crystal more frequently than they multiply, forcing other, harder sources of dislocations to be activated. Understanding and controlling the mechanical properties of materials on this scale may thus lead to new and more robust nanomechanical structures and devices.

ACKNOWLEDGMENTS

This work was supported by the Office of Science, Office of Basic Energy Sciences, of the U.S. Department of Energy under Contract Nos. DE-FG02-04ER46163 and DE-AC02-05CH11231. Additional support though an NSF-EU COLLABORATIVE RESEARCH PROGRAM: NANOMESO under NSF Grant No. 0502208 is gratefully acknowledged.

REFERENCES

[1] Arzt E., Acta Mater. 1998; 46: 5611

[2] Yu DY and Spaepen F, J. Appl. Phys. 2003; 95: 2991

[3] Nix WD, Metall. Trans. A 1989; 20A: 2217

[4] Stelmashenko NA, Walls MG, Brown LM, Millman YV, Acta Metall. Mater. 1993; 41: 2855

[5] De Guzman MS, Neubauer G, Flinn P, nix WD, Mater. Res. Soc. Proc. 1993: 308: 613

[6] Ma Q, Clarke DR, J. Mat. Res 1995; 10: 853

[7] Poole WJ, Ashby MF, Fleck NA, Scripta Mat. 1996; 34: 559

[8] Nix WD and Gao H, J. Mech. Phys. Solids 1998; 46: 411

[9] Gao H, Huang Y, Naturwissenschaftler 1999; 86: 507

[10] Gao H, Huang Y, Nix WD, Hutchinson JW, J. Mech. Phys. Solids 1999; 47: 1239

[11] Huang Y, Chen JY, Guo TF, Zhang L, Hwang KC, Int. J. Fract. 1999; 100: 1

[12] Huang Y, Gao H, Nix WD, J. W. Hutchinson, J. Mech. Phys. Solids 2000; 48: 99

[13] Huang Y, Xue, Gao H, Nix WD, Xia ZC, J. Mater. Res. 2000: 15: 1786

[14] Tymiak NI, Kramer DE, Bahr DF, Wyrobek TJ, Gerberich WW, Acta Mater. 2001: 49: 1021

[15] Swadener JG, George EP, Pharr GM, J. Mech. Phys. Solids 2002: 50: 681

[16] Durst K, Backes B, Goken M, Scripta Mat. 2005: 52: 1093

[17] Durst K, Backes B, Franke O, Goken M, Acta Mat. 2006: 54: 2547

[18] Basinski SJ and Basinski ZS, "Plastic deformation and work hardening," in Dislocations of Solids, Vol. 4: Dislocations in Metallurgy, edited by Nabarro FRN, North-Holland Publishing Company, Oxford, UK 1979: 261

[19] Uchic MD, Dimiduk DM, Florando JN and Nix WD, Science 2004; 305: 986

[20] Greer JR, Oliver WC and Nix WD, Acta Mater. 2005; 53: 1821; Greer JR, Ph.D dissertation, Stanford University 2005

[21] Greer JR and Nix WD, Phys. Rev. B 2006; 73: 245410

[22] Valek BC, Ph.D dissertation, Stanford University 2003

[23] Budiman AS, Tamura N, Valek BC, Gadre K, Maiz J, Spolenak R, Nix WD and Patel JR, App. Phys. Lett. 2006; 88: 233515

[24] Tamura N, MacDowell AA, Spolenak R, Valek BC, Bravman JC, Brown WL, Celestre RS, Padmore HA, Batterman BW & Patel JR, J. Synchrotron Rad. 2003; 10: 137

[25] Han SM, Ph.D dissertation, Stanford University 2006

[26] Cahn RW, J. Inst. Met. 1949; 86: 121

[27] Nye JF, Acta Metall. 1953; 1: 153

[28] Minor AM, Asif SAS, Shan ZW, Stach EA, Cyrankowski E, Wyrobek TJ, Warren OL, Nature Materials 2006; 5: 697

FIG. 1. The Au (111) film on Cr (200) substrate: (a) 4 variants of Au <111> out-of-plane crystals were observed in the planar view, as well as (b) through thickness of film (using ion beam contrast imaging inside an SEM at a 52° tilted angle); (c) Symmetric x-ray diffraction gave the Au (111) peaks of the film and the Cr (200) peak of the single crystal Cr substrate; however (d) non-symmetric x-ray diffraction (by tilting the sample 54.74° to get Au (200) peaks, and then scanning φ for 360°) gave 4 sets of three Au (200) peaks each separated by 120° angle, indicating the 4-crystal Au <111> film.

FIG. 2. The submicron Au pillar specimen; (a) the crater in the middle of which stands the pillar, with the identifying mark (number "4") on the left: SEM image, and (b) synchrotron white-beam X-Ray microFluorescence (XRF) scan; (c) a <111>-oriented gold pillar machined in the FIB (pillar diameter = 580 nm, pillar height = 1.9 μm (total) and ~ 1.1 μm (the upper crystal); a slight color contrast signifying differently oriented crystals between the upper and bottom crystals is visible upon careful inspection, as indicated by the arrows pointing to the interface).

FIG. 3. A schematic illustration of the synchrotron white-beam x-ray microdiffraction experiments (conducted at the ALS beamline 7.3.3, Lawrence Berkeley National Lab) on the Au submicron pillar on Cr substrate.

FIG. 4. A mapping of the $(\bar{3}11)$ Laue spot of the upper crystal of the pillar in the areas surrounding the pillar and the crater; step size = 1 μm. The dashed and dotted circle represents the 30 μm-crater, and as we expect, exactly in the middle of it, stands the pillar as marked by the rectangular solid line box.

FIG. 5. Stress-strain behavior of <111>-oriented Au single crystal submicron pillar: (a) flow stress increases significantly beyond its typical bulk values; (b) SEM image of a uniaxially compressed pillar after deformation.

FIG. 6. Side-by-side comparison between undeformed and deformed states of the pillar crystal; (a) SEM images of the Au pillar, (b) ($\bar{3}11$) Laue diffraction spots, and (c) quantitative analysis.

FIG. 7. (a) A particular configuration of edge dislocations of random signs (statistically-stored dislocations) might lead to lattice rotation as expressed in the formula; (b) Illustration of the geometry of our pillar – if spacing, *s*, between edge dislocations in (a) is larger than the dimensions of pillar crystal, then the pillar does not have enough space for such cells to exist.

Figure(s)

Click here to download high resolution image

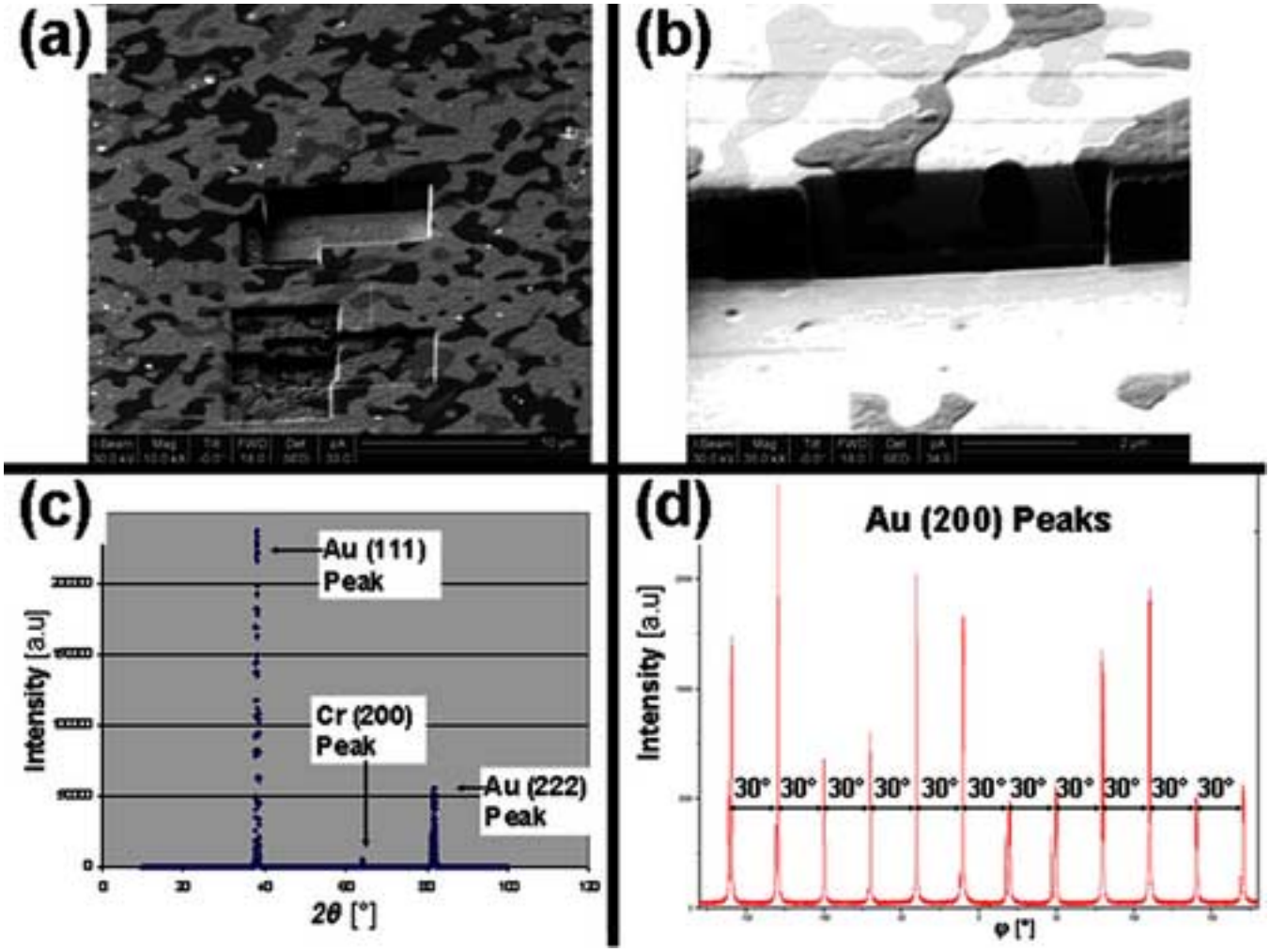

Figure(s)

Click here to download high resolution image

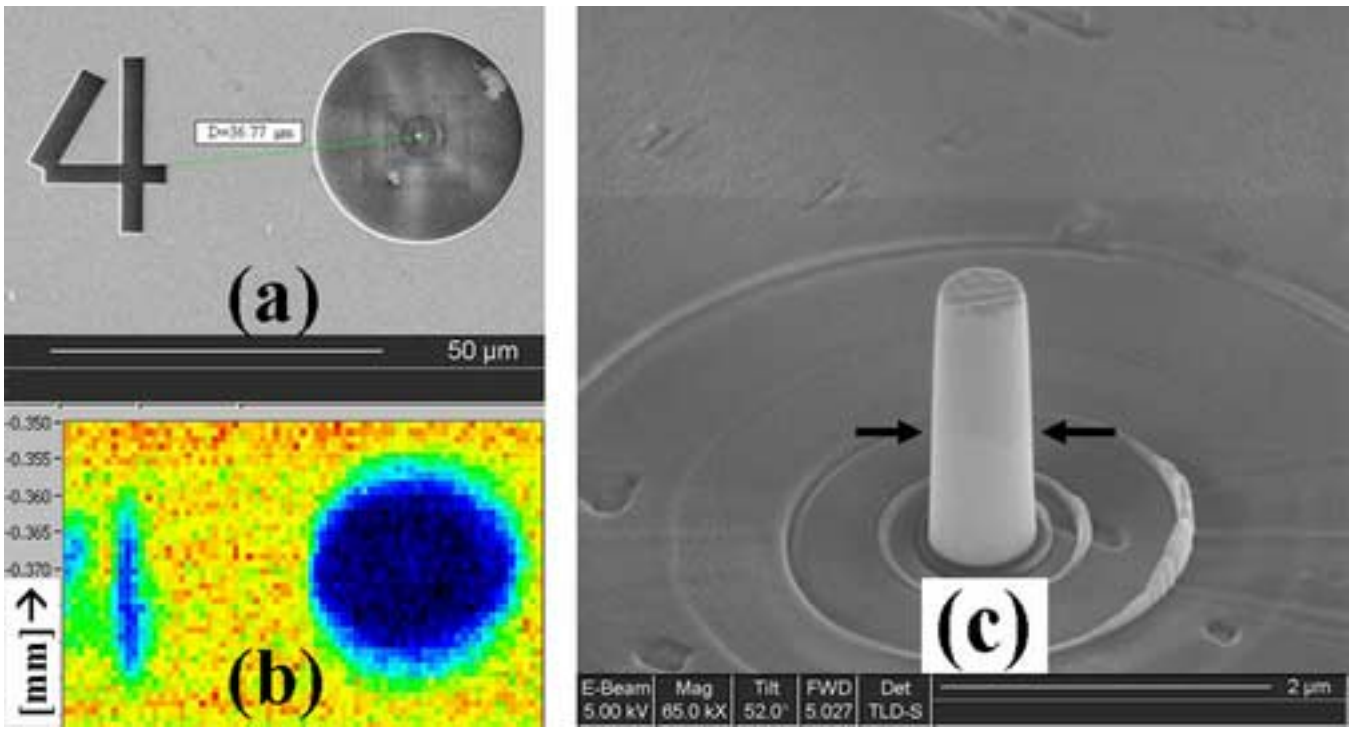

Figure(s)

Click here to download high resolution image

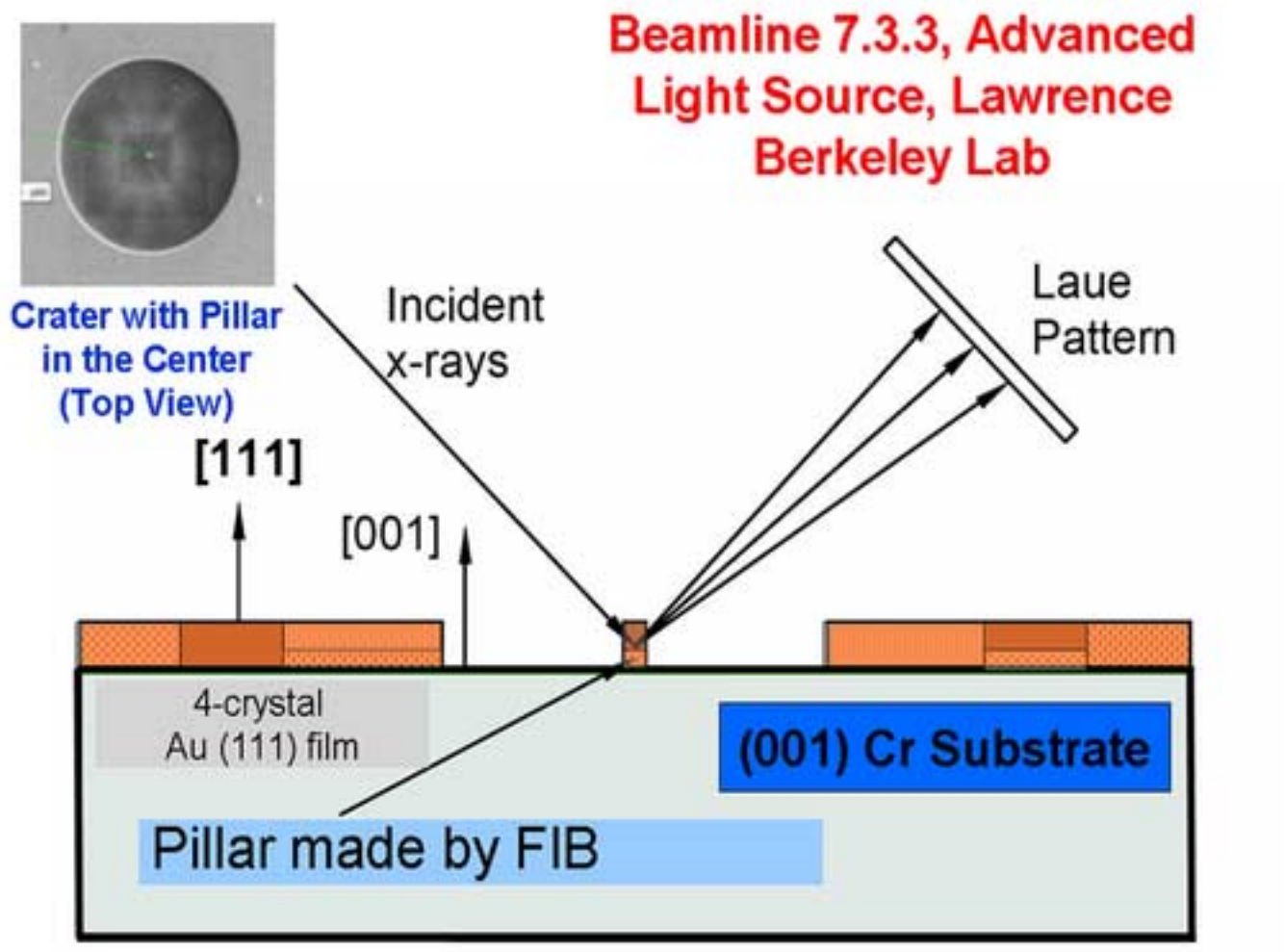

Figure(s)

Click here to download high resolution image

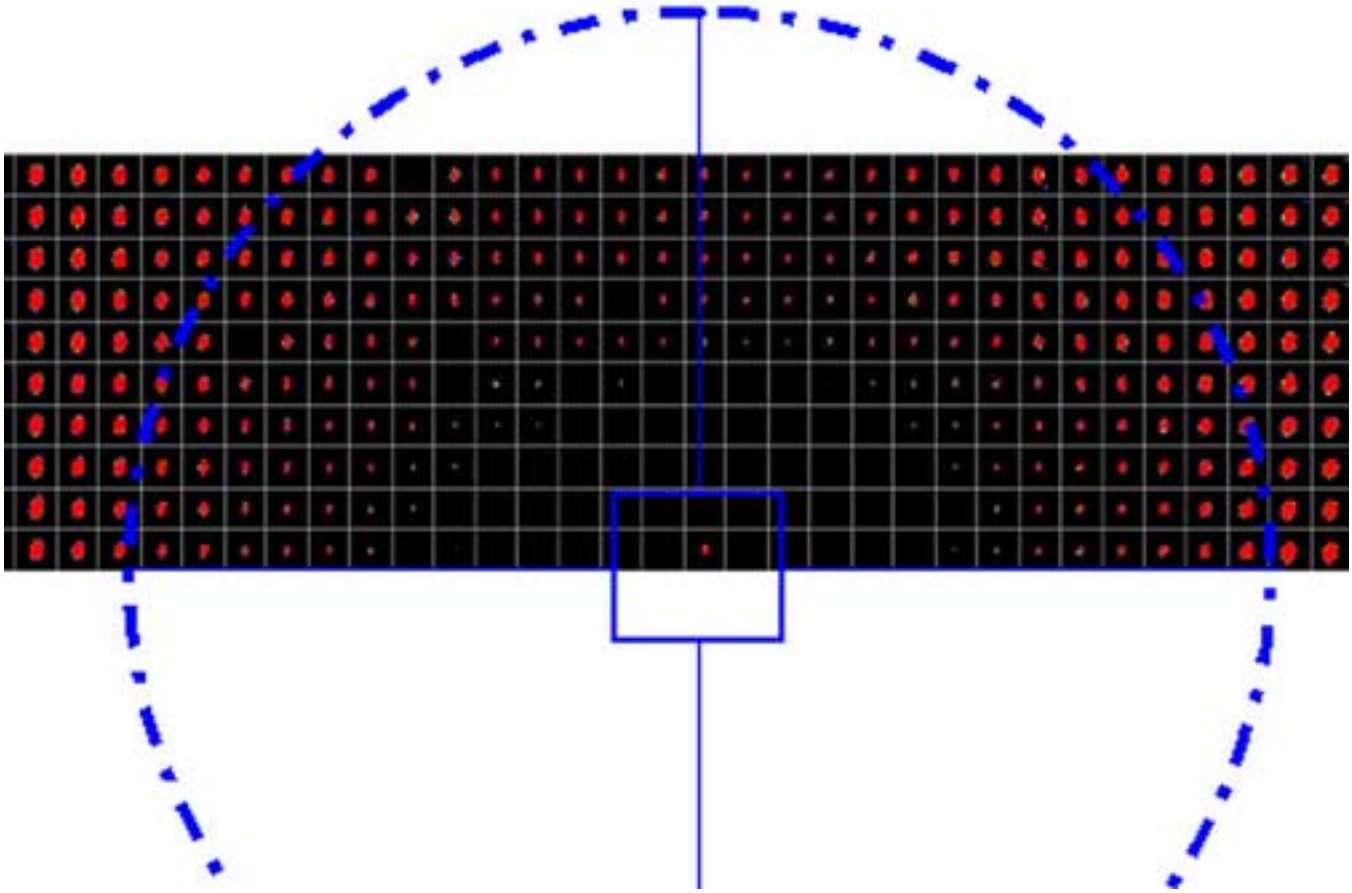

Figure(s)

Click here to download high resolution image

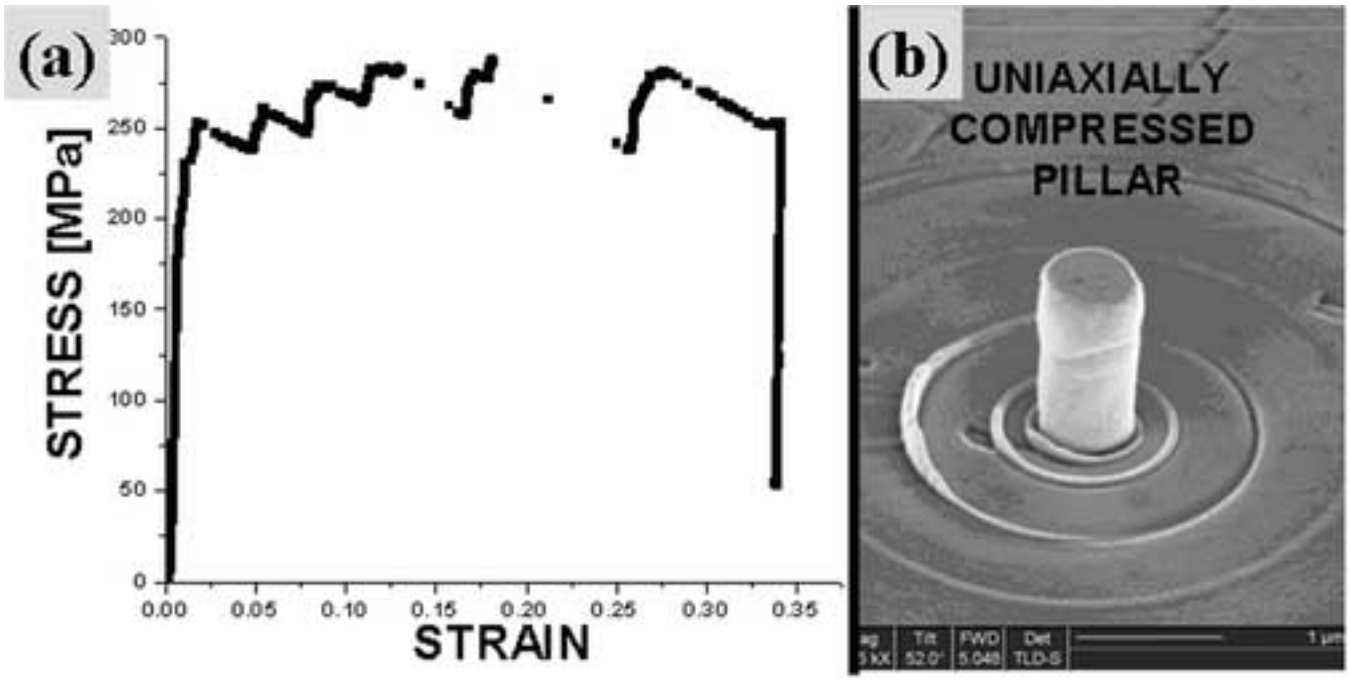

Figure(s)

Click here to download high resolution image

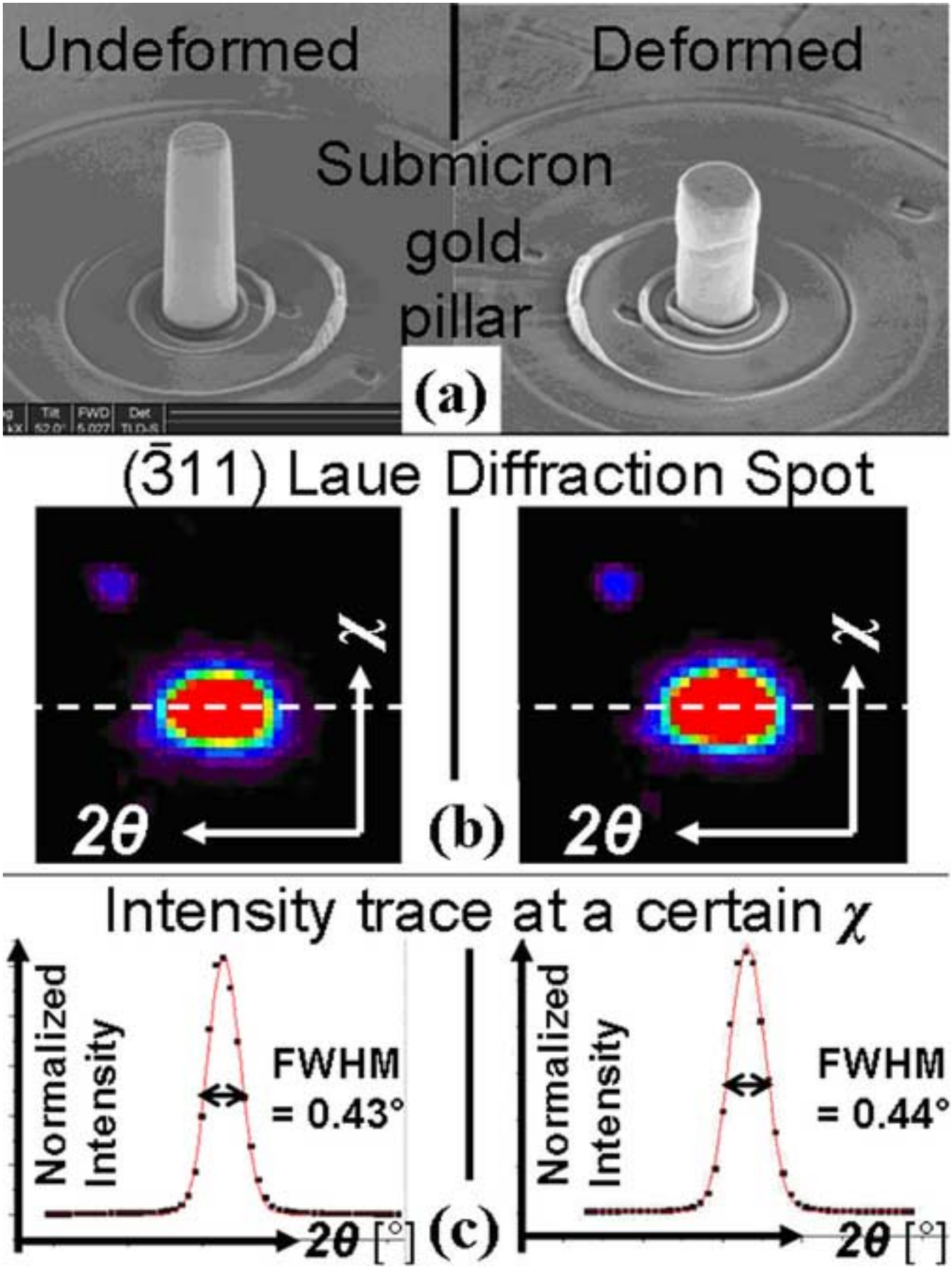

Figure(s)
Click here to download high resolution image